Liquid Crystals
Publication details, including instructions for authors and subscription information:
http://www.informaworld.com/smpp/title~content=t713926090

Multiple scattering of light from polymer dispersed liquid crystal material

Jaap H. M. Neijzen; Henk M. J. Boots; Frank A. M. A. Paulissen; Martin B. Van Der Mark; Hugo J. Cornelissen

Online publication date: 29 June 2010

To cite this Article Neijzen, Jaap H. M. , Boots, Henk M. J. , Paulissen, Frank A. M. A. , Van Der Mark, Martin B. and Cornelissen, Hugo J.(1997) 'Multiple scattering of light from polymer dispersed liquid crystal material', Liquid Crystals, 22: 3, 255 — 264
To link to this Article: DOI: 10.1080/026782997209306
URL: http://dx.doi.org/10.1080/026782997209306

LIQUID CRYSTALS, 1997, VOL. 22, NO. 3, 255–264

Multiple scattering of light from polymer dispersed liquid crystal material

by JAAP H. M. NEIJZEN, HENK M. J. BOOTS*,
FRANK A. M. A. PAULISSEN, MARTIN B. VAN DER MARK and
HUGO J. CORNELISSEN

Philips Research Laboratories, Professor Holstlaan 4, 5656 AA Eindhoven,
The Netherlands

(*Received 8 August 1996; accepted 7 October 1996*)

Light scattering from polymer dispersed liquid crystal (PDLC) material has been studied experimentally and by Monte Carlo simulation. Light scattering was measured as a function of both scattering angle and cell thickness. The cell thicknesses of practical interest are in an intermediate regime where neither single scattering nor light diffusion applies. Both the angular and the thickness dependence of the scattering intensity can be described accurately by a Monte Carlo simulation of multiple scattering from a homogeneous distribution of independent scatterers. The model smoothly interpolates between the single scattering limit for thin cells and the diffusion limit for thick cells. It can easily be extended to include any specific feature of a scattering display system.

1. Introduction

Over the past decade, cells containing nematic liquid crystal (LC) in a polymer matrix have become a viable alternative to twisted nematic cells in a number of applications. The most studied systems of this kind are polymer dispersed liquid crystals (PDLCs) [1–3]. In PDLCs, the polymer matrix is optically isotropic with a refractive index matching the ordinary refractive index of the liquid crystal in the dispersed phase. If no voltage is applied, the cell scatters light; if a sufficiently high voltage is applied across the cell, the director in the liquid crystalline droplets turns parallel to the field and the cell is transparent for perpendicularly incident light. Thus one may switch between a scattering off-state and a transparent on-state. Alternatively, the polymer matrix may be optically anisotropic such that all components of the dielectric tensor are the same for the matrix and for the liquid crystal. These systems, known as anisotropic gels [4], switch from a transparent to a scattering state on the application of a voltage.

Here we report experiments and Monte Carlo simulations on the thickness dependent angular distribution of light scattered from a PDLC slab in the off-state. In particular, we are interested in the dependence on layer thickness of what we will call the *contrast*. For the purpose of this paper we define contrast as *the inverse of the off-state transmittance within a small solid angle* $0 \leqslant \phi < 2\pi$, $0 \leqslant \theta < \theta_0$ *around the direction of the incoming beam*. Here $2\theta_0$ is the collection angle. If the device in the on-state were perfectly transparent, this definition would correspond to a genuine contrast ratio, applicable to PDLC shutters and projection displays, that is, the ratio between the transmittance in the on-state and the transmittance in the off-state, both within the collection cone. In this work, we do not consider the small corrections to perfect transmission in the on-state, which are due to haze, to reflections, and to light absorption in the conducting layers. Of these corrections, only the haze depends on thickness; it may be diminished by increasing the on-state voltage.

Most models for light scattering from PDLCs have concentrated on single scattering from spherical, ellipsoidal, or cylindrical LC 'droplets' [5–7]. Both the Rayleigh–Gans approximation for small droplets [5] and the anomalous diffraction approximation for large droplets with small birefringence [6], have been extended successfully to apply to droplets containing optically anisotropic material with a spatially varying director orientation. The results depend both on the shape of the droplets and on the director pattern within the droplet. Good agreement with experiment is found for the case of single scattering from isolated droplets.

In many practical systems, however, the LC content is high (typically 80 volume per cent) and multiple scattering is important [8, 9]. We will model multiple scattering of light as multiple scattering of particles. This restricts the model to situations where the wave-like nature of light is irrelevant; polarization effects, however,

* Author for correspondence.

can in principle be taken into account. It is common to call the particles photons, but one model photon does not correspond to one physical photon. The angular distribution of the intensity in a single scattering event (ADSE) is replaced by a probability distribution of scattering a photon into a certain direction. In the simulation of multiple scattering, one needs two probability distributions as *input*: (a) the distribution of distances between scattering events and (b) the angular distribution in a scattering event.

(a) For randomly positioned scatterers, the former distribution is exponential [10, 11]. The characteristic distance is called the scattering mean free path l_{scat}. It may be found from the experimental decay of the direct transmittance (the transmittance of unscattered light), so that it is not an adjustable parameter in the fitting of the scattering intensity.

(b) In many systems, the angular distribution in a scattering event (ADSE) is peaked around a scattering angle β of zero degrees. The average value of $\cos\beta$ is linked to a quantity called the transport mean free path, which is defined as $l_{trans} = l_{scat}/(1 - \langle\cos\beta\rangle)$ [12, 13]. It may be thought of as the typical distance a photon has to travel before the memory of its original direction is lost (compare the persistence length in the field of polymer chain statistics [14]). If the sample thickness d is much larger than l_{trans}, the only relevant parameter in the scattering process is l_{trans}; in this regime the transport of light may be described by a diffusion equation. For $d < l_{trans}$, the whole shape of the ADSE is of importance.

The primary *output* of the simulation is the external angular distribution of light leaving the sample after an arbitrary number of scattering events and of reflections and refractions at the slab surfaces.

The application of a Monte Carlo model in the study of multiple light scattering is not new. Such a model has been used in the recent past by a number of authors to verify new analytic theories of multiple scattering and to study complex multiple scattering systems that cannot be treated by analytic methods [13–15]. Monte Carlo methods tested on simple geometries can easily be extended to treat all kinds of specificities of complete devices of practical interest.

Kelly and Wu [9] were the first to simulate multiple light scattering from a PDLC by a Monte Carlo model. Their model has two input parameters: the scattering mean free path and the radius of the spherical droplets in their PDLC material. They do not actually trace the paths of scattered photons in their simulation, but approximate the pathlength in the PDLC slab by the thickness of the slab. Therefore their model is restricted to a rather common situation where the distribution of multiply scattered light is very narrow ($d \ll l_{trans}$). Refraction and reflection at the surfaces of the slab are not taken into account.

In the following two sections, the experiments and the model are described in detail. Then the experimental results are interpreted with the help of Monte Carlo simulation. A discussion concludes the paper.

2. Experimental

The dependence of scattering properties on layer thickness has been investigated using wedge shaped PDLC cells. The precise value of the cell gap as a function of the position in the cell was first measured on the empty cells by use of interferometry. After the filling and curing, these measurements were repeated for a limited number of positions, to allow for a final correction.

The PDLC layers investigated consisted of 80% TL205 and 20% PN393 supplied by Merck Ltd. The PDLC samples were UV-cured (13 mW cm^{-2} around $\lambda = 365$ nm) at temperatures of 25°C (wedge A) and 15°C (wedge B). Different curing temperatures resulted in PDLC layers with different scattering properties.

The experimental arrangement to measure the scattering distribution of a PDLC layer is schematically indicated in figure 1. A collimated beam of light originating from a halogen light source illuminates the PDLC sample. The beam diameter at the measuring spot is 1·5 mm. The divergence of the incoming beam is $\pm 0{\cdot}5°$. A green bandpass filter with a central wavelength of 560 nm and a full width at half maximum (FWHM) of 20 nm was used for most of the measurements. For

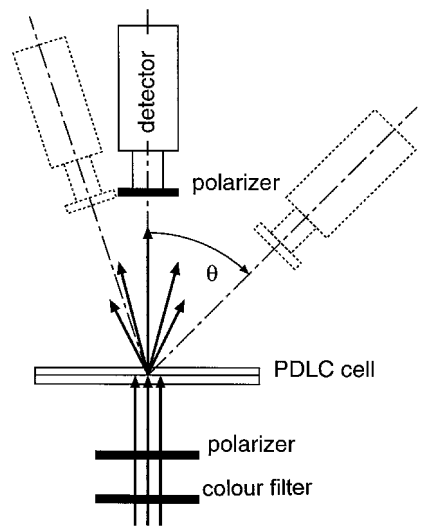

Figure 1. The experimental set-up.

the investigation of the wavelength dependence of the scattering distribution, bandpass filters with central wavelengths of 490, 550 and 630 nm (FWHM = 10 nm) were used. The angular distribution of the light scattered from the centre of the illuminated area is determined by a measuring microscope rotating around the measuring spot. Polarizers can be inserted in the incoming beam of light and in front of the microscope to determine the scattering distribution as a function of the polarization. The field of view of the microscope at the measuring position is a disc perpendicular to the optical axis of the detection unit, with a diameter of 0·25 mm. The collection half-angle, θ_0, of the detection system which samples the scattering distribution, is adjusted to $\theta_0 = 1°$ for the measurements of the angular dependence. The microscope actually measures the luminance of the illuminated PDLC area as a function of the polar angle θ. A luminous intensity distribution (lumen sr^{-1}) is obtained by multiplying this result by $\cos\theta$ and dividing it by the solid angle of the collection cone. The factor $\cos\theta$ compensates for the fact that the actual area from which scattered light is detected increases with increasing θ. Dividing this result by the incoming luminous flux yields a normalized luminous intensity with the dimension of 1/steradian (sr^{-1}). This normalized luminous intensity is the transmittance per steradian of the originally incident flux in the scattering direction θ. This will be referred to as the scattering distribution of the sample. Integration of this quantity over the total solid angle of 4π yields a value of 1.

The same experimental arrangement was used to determine the transmittance of the incident light in the forward direction ($\theta = 0$), integrated over a certain collection angle. A collection half-angle $\theta_0 = 2{\cdot}6°$ was used here. The divergence of the incoming beam was adjusted to $\pm 1°$ for these forward transmittance measurements.

A typical result for a scattering distribution of a 5 μm PDLC layer (wedge A), measured with a collection half-angle of 1°, is shown in figure 2. The incident beam was s-polarized (perpendicular to the scattering plane). The scattered light was detected in both the s- and p-polarizations (perpendicular and parallel to the scattering plane, respectively). In the scattering distribution obtained with both polarizers perpendicular to the scattering plane, two distinct contributions can be distinguished. The first contribution is a narrow peak around $\theta = 0$ which is the fraction of the original incident beam that has passed the PDLC film without scattering. This contribution, which will be referred to as 'direct transmittance', is still fully polarized, of course. The second contribution is a broad scattering distribution resulting from single and multiple scattering of incident light. The degree of depolarization in this scattering background is remarkable. This is true even for our thinnest samples,

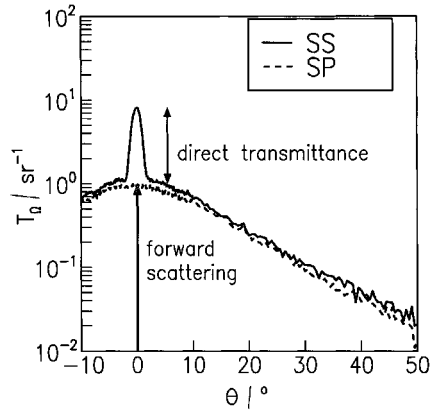

Figure 2. Typical scattering distribution for a 5 μm PDLC slab, measured in two polarization directions. The incident beam of light was s-polarized and both the s- and p-polarized scattered light was detected.

where small-angle scattering is dominated by single scattering. The conclusion is that even after only one or two scattering events, the memory of the initial polarization is virtually lost. The strong depolarization would not be expected for optically isotropic scatterers, but it is a well-known phenomenon in, for example, light scattering from a nematic LC. The small differences generally observed between the scattering distributions for the various orientations of the polarizers also indicate a low level of residual orientation of the PDLC material. Some spots in the wedges show stronger residual orientation in the scattering state. This has been considered as an artefact and has not been investigated in detail.

From the point of view of application of PDLC in scattering projection displays or shutters, the most interesting feature of the PDLC scattering distribution is the transmittance value around $\theta = 0$, and its dependence on layer thickness. The strong depolarization of the scattering background makes it easy to discriminate between direct transmittance and forward scattering at $\theta = 0$. It is not necessary to measure the complete distribution; transmittance measurements with parallel and crossed polarizers are sufficient. For both contributions to the transmittance in the forward direction, the relation with layer thickness has been evaluated experimentally.

For homogeneous layers, the direct transmittance value is expected to decay exponentially with increasing PDLC layer thickness. The dependence on layer thickness has been investigated using the wedge shaped PDLC samples (wedge A and wedge B). Figure 3 shows the results for the direct transmittance, which is the integral of the direct transmittance per steradian at $\theta = 0$ over the collection cone. For $\theta = 0$, all directly transmitted light is collected, since the divergence of the incident light is adjusted to be smaller than the collection angle. The direct transmittance peak can be pronounced, in

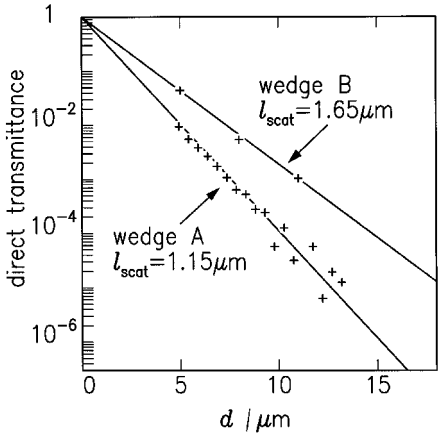

Figure 3. Measured decay of the direct transmittance with cell thickness d for wedges A and B. Experimental results are indicated by +; exponential fits with l_{scat} as a parameter are plotted as straight lines.

comparison with the broad scattering background, by using a small collection angle and a low divergence of the incident light. This makes it easier to measure the decrease of the direct transmittance over a number of decades. The exponential (Lambert–Beer) decay with slab thickness indicates that the material in the wedge is statistically homogeneous. The decay length in this plot yields a value for the scattering mean free path l_{scat}. The results for wedge A and wedge B are $l_{scat}=1{\cdot}15\pm0{\cdot}10\,\mu m$ and $l_{scat}=1{\cdot}65\pm0{\cdot}10\,\mu m$, respectively. The error is an estimate of the experimental uncertainties rather than the standard deviation of the data in figure 3.

3. Simulation

A model photon enters the slab at a certain angle (in this work perpendicularly). Part of it is reflected and part is transmitted according to the laws of Snel and Fresnel. The transmitted part (a photon with reduced statistical weight) travels a distance randomly taken from an exponential distribution with decay length l_{scat}, before it is scattered. Then it is scattered into a direction randomly taken from a given distribution of scattering angles β. This process is repeated until the photon hits one of the slab boundaries. At the slab boundary, part of it is refracted and leaves the slab at some angle θ. The other part is reflected according to the laws of Snel and Fresnel. Since we find experimentally that the original polarization is lost after only a few scattering events, we average the Fresnel laws for refraction and reflection over the polarization directions. The path of the photon is followed until the photon has been scattered 100 000 times or its weight has decreased below 0·0001. Statistical averaging was done over typically 2 000 000 photons.

The glass covers at the top and bottom sides of the wedges were modelled as scatter-free layers, displacing the points of reflection and refraction from the PDLC surfaces to the glass–air interfaces. This implies that we assumed that there is no refractive index mismatch between the polymer matrix and the glass covers.

In the model, the distribution of scattering directions $\hat{k}_s$ in a scattering event depends only on the direction $\hat{k}_i$ before scattering. (Here $\hat{k}$ indicates a unit vector in the direction of the wavevector k.) This describes scattering from an optically isotropic object, or the statistical average of scattering from an optically anisotropic object with a randomly oriented optical axis. The azimuthal angle of $\hat{k}_s$ around the direction $\hat{k}_i$ is uniformly distributed and the distribution of the angle β between $\hat{k}_s$ and $\hat{k}_i$ is chosen such that the experimental data are approximately reproduced by the simulation. Technically, the scattering direction was chosen by first choosing a random vector on the unit sphere according to the Marsaglia scheme [16] (to avoid time-consuming trigonometry). This yields a uniform distribution of $\cos\beta$ values between -1 and 1, which is reshaped to the desired distribution according to standard methods. For details, see [17].

The model was tested against analytic results for isotropic scattering ($l_{trans}=l_{scat}$) from slabs of refractive index 1 and 1·5 in vacuum. Perfect agreement was obtained.

4. Comparison between experiment and simulation

In order to compare the experiments with Monte Carlo simulations of multiple scattering, we have to supply two probability distributions: the distribution of distances between scattering events and the ADSE. From the experiment, we find an exponential decay of the direct transmittance with distance (Lambert–Beer), characterized by a certain value of l_{scat} (see figure 3); this distribution is used in the simulation as the distribution of distances between scattering events. As for the ADSE, we found good agreement with the experiments if we used a Lorentzian function of $(1-\cos\beta)$:

$$L(1-\cos\beta)\propto 1/[1+a^2(1-\cos\beta)^2], \qquad (1)$$

Here a determines the width of the distribution; the relation between a and l_{trans}/l_{scat} is calculated numerically. The value of l_{trans}/l_{scat} is adjusted such that the Monte Carlo results on the contrast fit the experimental results. We postpone the important discussion of other functional dependences of the ADSE on the angle β to §5 and limit ourselves here to simulation results from a Lorentzian and a Mie ADSE.

In Figures 4(*a*), 4(*b*) and 5, the observed scattering distribution and contrast are compared with the same quantities calculated from a simulation. For wedge A, good agreement is obtained for $l_{trans}/l_{scat}=50\pm5$; for

wedge B we find $l_{trans}/l_{scat}=45\pm5$. The deviation at small angles in figure 4 is largely due to the fact that in the experiment, the direct transmittance is included, while it is left out in the Monte Carlo data in figure 4. In the model, the incident ray is perfectly perpendicular to the sample and a more precise modelling of the divergence of the incident beam has not yet been attempted. In the calculation of the contrast, which involves an integration over a solid angle that is larger than the beam divergence, the direct transmittance is accounted for in the results from both the experiment and the simulation. In figures 4(*a*) and 5, we also include simulation results obtained when using a Mie distribution for the ADSE; they are not noticeably different from the results obtained using the Lorentzian. A Mie

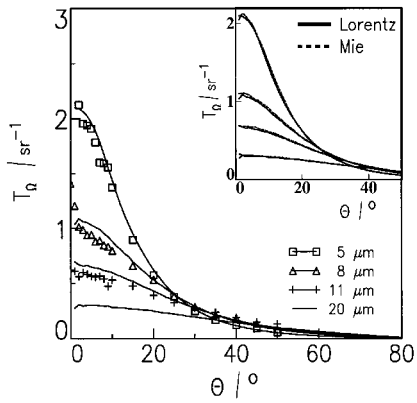

(*a*)

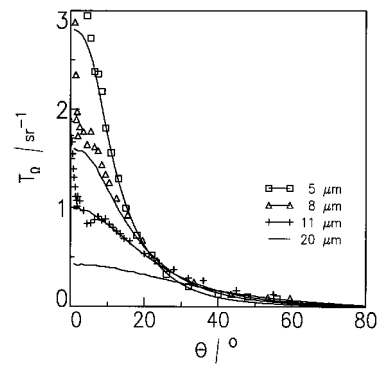

(*b*)

Figure 4. Angular distribution of scattered light: T_Ω, the transmittance per solid angle (or the normalized luminous intensity) as a function of scattering angle for some values of the cell thickness for wedges A (*a*) and B (*b*). Symbols indicate measurements: lines are the corresponding results from the simulation. In the inset we compare the angle-resolved luminous intensity from multiple scattering simulations using Lorentzian and Mie angular distributions in each scattering event. In the calculated intensities, the direct transmission is not included; in the measured intensities it is.

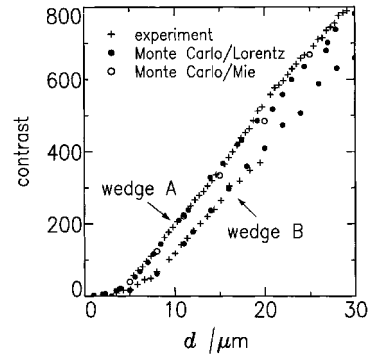

Figure 5. Contrast related to the luminous flux in a solid angle $0\leqslant\phi<2\pi$, $0\leqslant\theta<2{\cdot}6°$ around the direction of the incoming beam, as a function of PDLC thickness for both wedges. Measurements are compared with multiple scattering simulations using Lorentzian and Mie angular distributions in each scattering event. The slab is covered on both sides by glass plates of thickness 3 mm.

distribution with $l_{trans}/l_{scat}=50$ is obtained if we use monodisperse optically isotropic spheres of diameter 2·1 μm and a refractive index contrast between the spheres and the matrix of 0·14; with these parameters, we set the volume fraction of spheres equal to 0·4 in order to obtain $l_{scat}=1{\cdot}15$ μm. In the discussion in § 5, we will link these parameter values to the morphology as determined by confocal microscopy.

The wavelength dependence of the contrast is explored in figure 6; the data were obtained for wedge A. It turned out that at the time of measurement of these data, the scattering mean free path at a wavelength of 560 nm had changed to about 1·07 μm, while the ratio l_{trans}/l_{scat} was still about 50. In a Lorentzian ADSE, the only wavelength dependence is in the adjustable parameter a or, equivalently, in l_{trans}, but there is no model for this

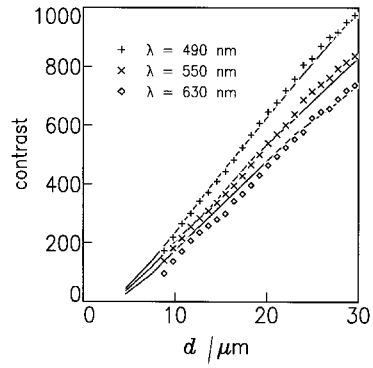

Figure 6. Contrast as a function of thickness at different wavelengths of the incident light. Experiment results are indicated by symbols. Lines are obtained by simulating multiple scattering from Mie spheres with a diameter of 2·1 μm at a volume fraction of 0·43. The refractive index difference is adjusted to 0·135 at 550 nm and was assumed to vary with wavelength in proportion to the birefringence.

dependence. Therefore we used multiple Mie scattering from monodisperse optically isotropic spheres in the Monte Carlo model. In the case of a Lorentzian ADSE, we have two parameters: l_{scat} and l_{trans}. In the case of a Mie ADSE, we have three adjustable parameters. Extensive parameter searches show that for scattering from monodisperse optically isotropic spheres, only one combination of parameter values (with a small spread) provides a good description of the thickness and wavelength dependence of the contrast: the diameter of the spheres is taken as 2·1 μm, the volume fraction of the spheres is taken as 0·43, and the effective refractive index mismatch Δn_{560} between spheres and matrix at a wavelength of 560 nm is taken to be 0·14. The results appeared to be quite insensitive to the precise value of the refractive index of the matrix within the range 1·5–1·7. Although the exact Mie formulae were used, we checked that in this range of parameter values, the anomalous diffraction approximation is allowed. It was assumed that the dispersion in the refractive index mismatch between spheres and matrix scaled with the known wavelength dependence of the birefringence of the LC [18]. The calculations showed that the dispersion in the contrast is largely due to the dispersion in the scattering mean free path, which could be adjusted by tuning the parameter Δn_{560}. From additional calculations we deduce that in order to maintain a good fit to the experimental wavelength dependence of the contrast for the case of *polydisperse* Mie spheres, the average diameter and the refractive index difference must be taken smaller than the values cited above.

5. Discussion

5.1. *Monte Carlo simulation between the limits of single scattering and diffusion*

The Monte Carlo simulations interpolate between two limits:

(1) If $d < l_{scat}$, the contrast is dominated by the attenuation of the unscattered light. In that case the contrast is approximately equal to the inverse of the direct transmittance, so that it increases exponentially with thickness.

(2) If $d \gg l_{trans}$, the scattering of light may be described as a diffusion process and a linear relation between contrast and thickness is expected [13].

In figure 7 we show that the experimental results for our PDLC layers of industrial interest cannot be described by either limit. However, the agreement with the simulation results is good.

The deviations of the simulation results from the Lambert–Beer law at $d > l_{scat}$ are similar to the experimental deviations reported by Yamaguchi and Sato [19]. They have interpreted these deviations as an apparent increase of the scattering mean free path due to boundary layer effects. However, multiple scattering of light provides an alternative explanation of their results.

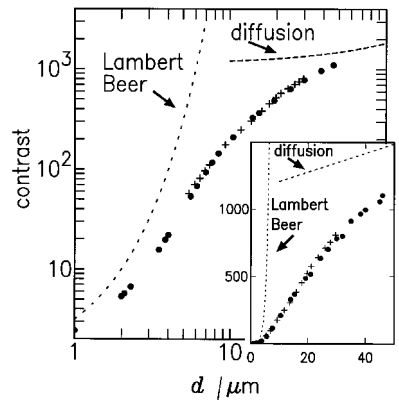

Figure 7. Log–log plot and linear plot (inset) of experimental (+) and Monte Carlo (●) results for wedge A, given earlier in figure 5. The dashed line indicates the linear relation between contrast and thickness in the diffusion limit ($d \gg l_{trans}$) and the dotted line indicates the Lambert–Beer decay of the direct transmission which dominates the contrast for $d < l_{scat}$.

One may be tempted to associate linear relationships between contrast and thickness with the diffusion regime. However, the curves in figure 5 are smooth and parts of the curves may be approximated by straight lines, even though it is clear from figure 7 that the diffusion limit has not yet been reached. Any such linearization holds over a limited range of thickness values and lacks a physical basis. This holds also for the proportionality between contrast and thickness that figure 5 suggests for $20\,\mu m < d < 30\,\mu m$. For their system, Tomita and Jones [20] report such proportionality for $10\,\mu m < d < 16\,\mu m$ and they use this observation in their definition of a figure of merit, which in our view can be of use only in a limited range.

5.2. *Dependence of contrast on collection angle*

The simulation results in figure 8 pertain to three values of the collection half angle θ_0 and to the cases of scattering layers with and without non-scattering cover glasses. It is clear that the direct transmittance (which leads to the Lambert–Beer curve in figure 8) will not depend on the collection angle if the divergence of the incoming beam is small enough. The transmittance due to forward scattering, on the other hand, does depend on the collection angle. Since the broad scattering distribution is approximately constant for small collection angles, the contrast will vary quadratically with θ_0 (for small θ_0). So the contribution due to forward scattering

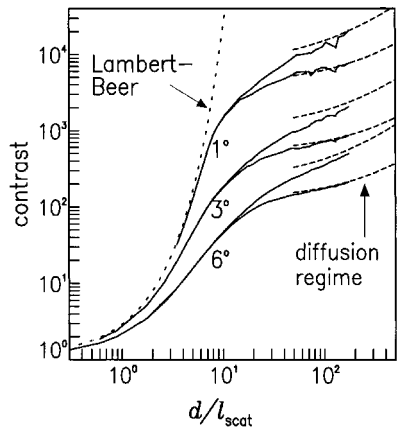

Figure 8. Monte Carlo results of the contrast as a function of d/l_{scat} for a material characterized by $l_{trans}/l_{scat}=50$ and $l_{scat}=1{\cdot}15\,\mu m$. Three pairs of curves are shown, pertaining to the luminous flux in a solid angle $0\leqslant\phi<2\pi$, $0\leqslant\theta<\theta_0$ around the direction of the incoming beam, with $\theta_0=1°$ (upper pair of curves), 3° (middle pair) and 6° (lower pair). The upper curve in each pair corresponds to a beam width with a diameter of 1·5 mm and to a PDLC slab covered with 3 mm glass plates on both sides; the lower curve corresponds to the case of an infinitely wide incident beam or to an uncovered PDLC slab. Dashed lines indicate the diffusion limit ($d\gg l_{trans}$). The short dashes indicate the Lambert–Beer decay of the direct transmission ($d< l_{scat}$).

may be reduced by reducing the collection angle, while the contribution of the direct transmittance can be reduced only by improving the scattering properties of the PDLC material or by increasing the layer thickness.

5.3. *The influence of cover glasses*

In the experiment, the cell is covered with thick (3 mm) glass plates. These are taken into account in the simulation. Light that is reflected at the glass–air interface at a large angle with the normal, will be displaced over a distance of the order of millimetres before it enters the scattering region again. Therefore, a significant part of the light may leave the sample well away from the illuminated spot and well away from the region from which the scattered light is collected. A more detailed analysis shows that the relevant parameter for the importance of glass covers is the ratio between the glass thickness and the width of the illuminated spot. Such effects are of importance in assessing the amount of optical cross-talk in displays. Figure 8 shows that in our experimental configuration, the glass plates have an important effect on the contrast of thick scattering cells. In this figure, the upper curve at each collection angle pertains to the covered PCLC layer, while the lower one pertains to the bare layer. The effects of cover glasses have been described more qualitatively before [21], but through our Monte Carlo model we can quantify the effect for any specific display system.

5.4. *The relation between morphology and scattering model*

Interpretation of our experiments by multiple Mie scattering yielded a sphere size of 2·1 μm, a refractive index contrast of 0·14 and a volume fraction of 0·43. In this section we discuss the relation between these model parameters and the morphology of the PDLC material.

In figure 9, we show a confocal microscopy picture of a sample that has been cured under circumstances that are insignificantly different from the curing conditions of wedge A [21A]. It is seen that in our PDLC material, LC droplets are densely packed. Scattering is between droplets of different orientation rather than between a droplet and the medium. Thus, we should identify the medium in the calculations not with the polymer matrix, but with the average effect of droplets of random orientation. Therefore, the volume fraction of the effective medium found from the simulation is much higher than the volume fraction of the polymer matrix between the LC droplets. Similarly, the difference between the effective refractive index contrast of 0·14 and the LC birefringence of 0·22 arises from the fact that scattering is between droplets of random orientation; therefore the

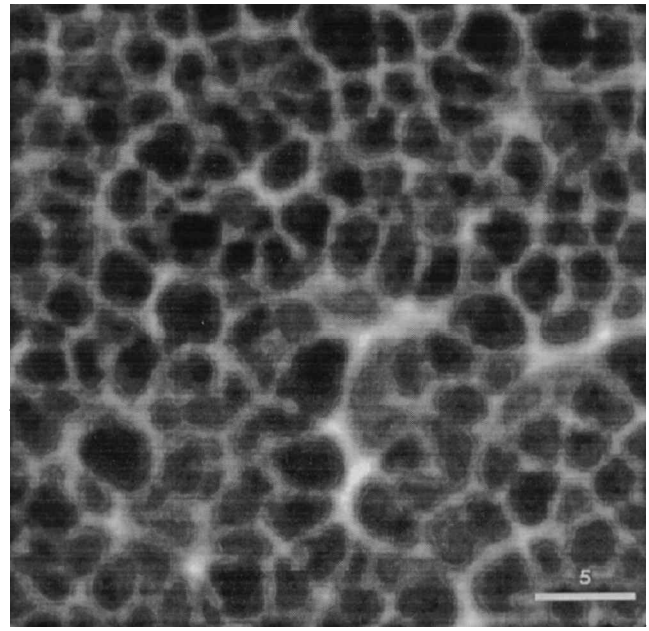

Figure 9. Confocal microscopic cross-section in the middle of the cell parallel to the cell walls. The figure was produced by K. Amundson, A. van Blaaderen, and P. Wiltzius at AT and T Bell Laboratories, Murray Hill. Their PDLC material differs only in the curing conditions (22°C, 17 mW cm^{-2}) from the wedge A material; such differences are insignificant [21A].

maximal refractive index mismatch occurs only in few places.

The typical droplet size of 2–3 μm in figure 9 does agree with the Mie sphere diameter of 2·1 μm. We should emphasize, however, that such comparison can only be qualitative: the droplets are not perfectly spherical and the director pattern in each droplet may be intricate. In the Mie model we disregarded these complications; the director pattern is not known and a multiple scattering model that includes scattering between droplets with different director patterns would be far less tractable. We do believe, however, that a comparison between the morphology and a multiple Mie scattering interpretation of light scattering will be useful in the interpretation of the effects of systematic variations in morphology. To illustrate this point, we show in figure 10 the variation of contrast with the Mie sphere diameter; the same trend is expected for the variation of contrast with droplet size. In this comparison we kept the volume fraction and the ratio between the diameter and the cell thickness constant. This ratio is kept constant, since it is in practice undesirable to increase contrast at the expense of an increase in switching voltage. The switching voltage across a single sphere is independent of the sphere diameter and the spheres are densely packed (see figure 9) so that the switching voltage across the cell will be invariant if the diameter and the cell thickness change by the same factor. Figure 10 shows that in our material a sphere diameter of 2–3 μm gives the best contrast.

However complicated the morphology of a material may be, the main features of light scattering are determined by the two characteristic length scales l_{scat} and l_{trans}. The success of our simple model for small and large thicknesses, originates from the fact that it contains these two parameters, which are extracted from experiment. The success of the model at intermediate thicknesses is more surprising: in this regime, not only the two length scales are of importance, but also the functional form of the ADSE. This point is discussed below.

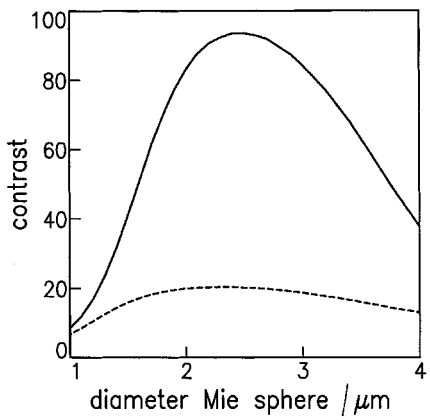

Figure 10. Contrast as a function of Mie sphere diameter at collection half-angles of 2·6° (top) and 6° (bottom) for a volume fraction of 0·4 of scattering spheres and a diameter/thickness ratio of 0·3.

5.5. *Different functional forms of the ADSE*

In order to judge the dependence on the functional form of the ADSE we tried not only Lorentzian and Mie distributions, but also a Gaussian in β [9],

$$G(\beta) \propto \exp(-b\beta^2), \tag{2}$$

and a Henyey–Greenstein distribution [22],

$$H(\cos\beta) = \frac{1}{2}(1-g^2)(1+g^2-2g\cos\beta)^{-3/2}. \tag{3}$$

The Henyey–Greenstein ADSE has often been used in multiple scattering studies because of its convenient analytical properties. Moreover, we tried a Gaussian and an exponential in $(1-\cos\beta)$. In equations (2) and (3), b and g determine the width of the distribution; the relation between b and l_{trans}/l_{scat} is calculated numerically, whereas $g = \langle\cos\beta\rangle = 1 - l_{scat}/l_{trans}$. In figure 11 (*a*), a normalized Lorentzian function of $(1-\cos\beta)$ is compared with two normalized Gaussian functions of β. The peak of the Gaussian function with $l_{trans}/l_{scat} = 120$ is similar to the peak of a Lorentzian with $l_{trans}/l_{scat} = 50$, while the peak of the Gaussian function with $l_{trans}/l_{scat} = 50$ is much broader and lower. Note that the ratio l_{trans}/l_{scat} is inversely proportional to $1 - \langle\cos\beta\rangle$. Therefore figure 11 (*a*) shows that a Gaussian that is close to a Lorentzian near the peak, differs strongly from it at the first moment of the distribution. A similar comparison between a Lorentzian and a Henyey–Greenstein distribution is shown in figure 11 (*b*). Van de Hulst [23] has emphasized the far-reaching consequences of differences in wing shape between different choices for the ADSE. The decay of a Gaussian is much faster and the decay of a Henyey–Greenstein function is much slower than the decay of a Lorentzian. Thus we may fit different ADSE functions to single scattering data (scattering data from *thin* PDLC layers) if we may freely adjust the value of l_{trans}/l_{scat}. However, for *thick* PDLC layers with strong multiple scattering, the functional form of the ADSE is immaterial and the transport mean free path is the only important parameter. Our procedure was first to determine l_{trans} by comparing Monte Carlo and experimental results for thick cells and then to judge which distribution described by that l_{trans} yielded a good agreement between simulation and experiment for thin cells. The important conclusion was that, of all distributions that we tried, only the Lorentzian and Mie distributions performed well.

It is a question of fundamental and practical interest how general the validity is of a Lorentzian ADSE. For

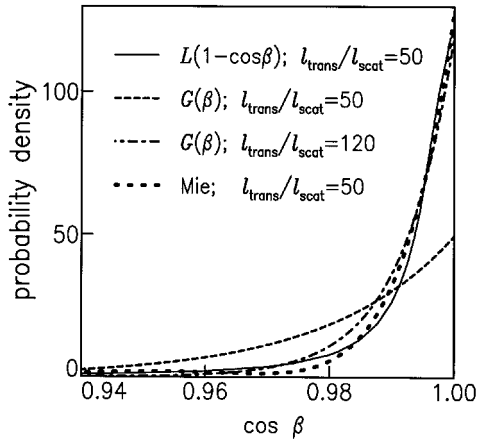

(*a*)

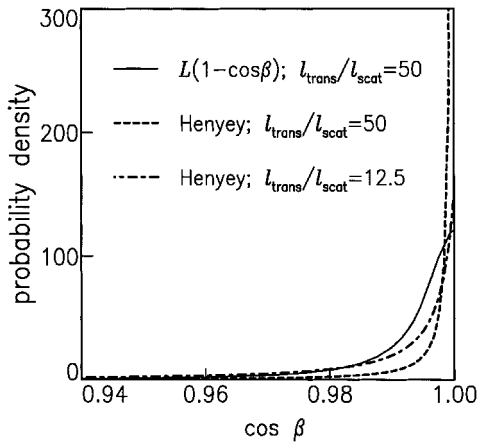

(*b*)

Figure 11. Comparison of probability distributions: a Lorentzian in $(1-\cos\beta)$, denoted as $L(1-\cos\beta)$, two Gaussians in β, denoted as $G(\beta)$ (*a*), a Mie distribution (*a*) and two Henyey-Greenstein distributions (*b*). The Gaussian and the Henyey–Greenstein functions that are close to the Lorentzian in the peak, have values of l_{trans}/l_{scat} that differ strongly from the value 50 that was used for the Lorentzian. All distributions P are normalized such that $\int_{-1}^{1} P \mathrm{d}\cos\beta = 1$. The Mie distribution is calculated for optically isotropic spheres of diameter 1·98 μm and of refractive index 1·65 in a medium of refractive index 1·52. It is sensitive only to the refractive index mismatch and the sphere diameter.

$l_{trans}/l_{scat} = 50$, we compared Lorentzian and Mie distributions and found a close similarity (see figure 11 (*a*)). Moreover, we found good agreement between simulation results of a simple model using a Lorentzian or a Mie ADSE and experimental results on our complex PDLC material (see figure 4 (*a*)). As yet, this is not sufficient evidence to conclude that a Lorentzian ADSE is typical of all strongly scattering PDLC materials. A study of this issue would be of great importance to anyone who is interested in simulating multiple scattering from PDLC systems.

6. Conclusion

In conclusion, we have shown that a simple Monte Carlo model based on independent, homogeneously distributed, optically isotropic scatterers is able to describe multiple scattering from structurally complicated PDLCs as a function of scattering angle and cell thickness. The agreement between simulation and experiment is good if we use a Lorentzian function of $(1-\cos\beta)$ or a Mie function for optically isotropic droplets as the angular distribution function in each single scattering event, but large discrepancies occur if we use Gaussian, exponential, or Henyey–Greenstein distribution functions. The sphere diameter in the Mie function is consistent with the droplet size as found from confocal microscopy. The PDLC cells under consideration can be described by neither direct transmission only and single scattering, nor by pure diffusive transport of light. The model bridges the gap between these limits. It can easily be extended to predict the properties of more complicated display systems involving a scattering cell in combination with layers and masks with known optical properties.

We wish to thank Karl Amundson, Alfons van Blaaderen and Pierre Wiltzius for allowing us to make use of their unpublished result, figure 9. We also thank P. Nolan (Merck Ltd) for providing us with the polymer and LC materials and for information on the wavelength dependence of the refractive indices of their materials. Furthermore we gratefully acknowledge stimulating discussions with H. C. van de Hulst, S. J. Picken and P. den Outer.

References

[1] Doane, J. W., Golemme, A., West, J. L., Whitehead, J. B., and Wu, B.-G., 1988, *Mol. Cryst. liq. Cryst.*, **165,** 511.
[2] Kelly, J. R., and Palffy-Muhoray, P., 1994, *Mol. Cryst. liq. Cryst.*, **243,** 11.
[3] Drzaic, P. S., 1995, *Liquid Crystal Dispersions* (Singapore: WorldScientific).
[4] (*a*) Hikmet, R. A. M., 1990, *J. appl. Phys.*, **68,** 406; (*b*) Hikmet, R. A. M., and Boots, H. M. J., 1995, *Phys. Rev. E*, **51,** 5824, and references therein.
[5] Žumer, S., and Doane, J. W., 1986, *Phys. Rev. A*, **34,** 3373.
[6] Žumer, S., 1988, *Phys. Rev. A*, **37,** 4006.
[7] Kelly, J. R., Wu, W., and Palffy-Muhoray, P., 1992, *Mol. Cryst. liq. Cryst.*, **223,** 251.
[8] Montgomery Jr., G. P., 1988, *J. opt. Soc. Am. B*, **5,** 774.
[9] Kelly, J. R., and Wu, W., 1993, *Liq. Cryst.*, **14,** 1683.
[10] A. Ishimaru, 1978, *Wave Propagation and Scattering in Random Media* (New York: Academic Press).

[11] Van de Hulst, H. C., 1980, *Multiple Light Scattering: Tables, Formulas, and Applications* (New York: Academic Press).
[12] Van de Hulst, H. C., 1957, *Light Scattering by Small Particles* (New York: Wiley).
[13] Durian, D. J., 1994, *Phys. Rev. E*, **50,** 857.
[14] (*a*) Picken, S. J., Van Wijk, R. J., Lichtenbelt, J. W. T., Westerink, J. B., and van Klink, P. J., 1995, *Mol. Cryst. liq. Cryst.*, **261,** 535; (*b*) Picken, S. J., private communication.
[15] (*a*) Den Outer, P. N., 1995, *PhD thesis*, Universiteit van Amsterdam; (*b*) Bolt, R. A., 1995, *PhD thesis*, Rijksuniversiteit Groningen.
[16] (*a*) Marsaglia, G., 1972, *Ann. Math. Stat.*, **43,** 645; (*b*) Allen, M. P., and Tildesley, D. J., 1990, *Computer Simulation of Liquids* (Oxford: Oxford University Press).
[17] Kurdikar, D. L., Boots, H. M. J. and Peppas, N. A., 1995, *Macromolecules*, **28,** 5632.
[18] Nolan, P., (Merck Ltd, Poole, UK), 1996, private communication.
[19] Yamaguchi, R., and Sato, S., 1994, *Jpn. J. appl. Phys.*, **33,** 4007.
[20] Tomita, A., and Jones, P., 1992, *SID International Symposium Digest*, **23,** 579.
[21] Takahara, H., and Omae, H., 1994, European Patent Application 94106399.2.
[21A] Amundson, K., van Blaaderen, A., and Wiltzius, P., ['An Investigation of Polymer-Dispersed Liquid Crystals: Morphology and Electro-Optical Performance',] submitted to *Phys. Rev. E.*
[22] Henyey, L. G., and Greenstein, J. L., 1941, *Astrophys. J.*, **93,** 70.
[23] Van de Hulst, H. C., 1996, *Rev. mod. Astr.*, **9,** (to be published).
[24] Amundson, K., van Blaaderen, A., and Wiltzius, P., ['An Investigation of Polymer-Dispersed Liquid Crystals: Morphology and Electro-Optical Performance',] (to be published).